EFFECTS OF THE SECONDARY AGING T6I4 ON FRACTURE TOUGHNESS AND FATIGUE CRACK GROWTH RESISTANCE OF AA7050 ALLOY

Carlos A.R.P. Baptista[1], Ana M.B.S. Antunes[2], Luis R.O. Hein[3], Samara C. de Paula[2] and Gabriel C.C. Peinado[2]

[1] University of São Paulo, Engineering School of Lorena (carlos.baptista@usp.br)
[2] University of São Paulo, Engineering School of Lorena (EEL-USP), Brazil
[3] São Paulo State University, Faculty of Engineering and Sciences at Guaratinguetá (FEG-UNESP), Guaratinguetá/SP, Brazil

Abstract: The aim of this work was to evaluate the effects of T6I4 interrupted aging heat treatment on the fracture toughness and fatigue crack growth behavior of AA7050 plate samples. The alloy was supplied in the form of a 75 mm thick rolled plate in the commercial T7451 temper. The T6I4 condition was obtained from the as-received material by means of a solution treatment (485°C / 4h) followed by two-step aging (145°C / 30 min and 65°C / 24h). The fracture toughness of the material in both T7451 and T6I4 conditions was determined using the Chevron notch methodology. The fatigue crack growth tests were conducted under constant amplitude and variable amplitude loadings. In the former case, C(T) notched specimens were employed and the crack length was measured by the compliance method. In the latter case, the FALSTAFF spectrum loading of hourglass shaped specimens was adopted and the crack length was measured by quantitative fractography. The obtained results showed an expressive increase of the materials' K_{QvM} values for the T6I4 condition (58.4 MPa·m$^{0.5}$) compared to T7451 temper (39.3 MPa·m$^{0.5}$). The fatigue crack growth behavior of these material conditions under both constant and variable amplitude loadings was found to be nearly similar. However, the higher apparent threshold observed in the constant amplitude tests and higher fatigue life presented by the T6I4 specimen under spectrum loading lead us to conclude that this material condition is more prone to the transient notch effect that retards the initial growth of a nascent crack.

Keywords: AA7050 alloy, interrupted aging, fracture toughness, fatigue crack growth.

INTRODUCTION

Age hardened aluminium alloys have been extensively employed in the aerospace and automotive industries. Al-Mg-Zn-Cu alloys (7xxx series) are the standard materials for manufacturing aircraft wing components requiring a compromise between mechanical strength and fracture toughness [1, 2]. The mechanical properties of aluminum alloys depend on the interactions among chemical composition, microstructure, heat treatment and forming processes, in which dislocations and alloy elements are the most important factors for the hardening phenomena. The presence of particles creates barriers to dislocation movement, thus affecting the hardening rate and the slope of the stress-strain curve [3]. The intermetallic coarse particles formed during the solidification of the alloy do not affect yield and tensile

strength significantly; however, they reduce the alloy's ductility. On the other hand, the fine precipitates formed during aging heat treatments increase both yield and tensile strength and can act as crack nucleation sites during the fatigue process [4]. The strengthening response of age-hardenable aluminum alloys depends on the type, morphology, spacing, volume fraction and size of the fine precipitates [2].

The usual precipitation sequence of the 7xxx series alloys from the super-saturated solid solution can be represented as: solid solution → GPI and GPII zones → metastable η' → stable η ($MgZn_2$). Moreover, the η phase can show nine different orientation relationships with Al matrix, named η_1 to η_9 [2, 4-6]. The resulting precipitates depend on the temperature and time of aging and nucleation conditions. Commercial alloys based on the Al-Zn-Mg-Cu system have maximum strength when aged to the T6 temper (120-130°C) [2]. Generally, the pre-stretching is applied to 7xxx series alloys in the as-quenched state in order to relieve quench-induced internal stress. While the strength of these alloys can be increased through appropriate thermo-mechanical treatments, it is difficult to keep the fracture toughness at a high level simultaneously. The corrosion resistance is also poor for a peak aged alloy. Investigations have shown that the fracture toughness is influenced by a range of microstructural features, such as the coarse particles, aging precipitates, configuration of the precipitation free zone (PFZ) and the grain size. To increase the fracture toughness and stress corrosion cracking (SCC) resistance, over aging was developed. However, the strength of over aged 7xxx alloys is decreased by 5-10% compared to that of peak aged condition [7].

Alternative heat treatments have been proposed aiming to increase fracture toughness and corrosion resistance without reduction in strength. A three-step aging, termed retrogression and re-aging (RRA) offer relatively good strength levels combined with improved SCC resistance, but cannot be successfully applied to thick sections [2, 8]. Another method was then developed, the so-called interrupted aging T6I4 (I = interrupted), in which an alloy is underaged at temperature levels related to the T6 temper for a short period of time and then submitted to a secondary aging at a lower temperature range (e.g., 25-65°C) for an extended period of time. The T6I4-65 temper was shown to increase the density of η' platelets in AA7050 alloy compared to the T6 condition, and this was due to a gradual evolution of the spherical GPI zones formed in the initial stage (15 min at 130°C) of the treatment. It was assumed that the higher density of refined precipitates produced in T6I4-65 temper results in tensile properties comparable to those of T6 temper combined with improved fracture toughness [2, 9].

AA7050, which is the main subject of this work, is widely used in several aircraft. Typical applications of plates include fuselage frames and bulkheads, while AA7050 sheet is used for wing skins. In aircraft industry, the fracture toughness and fatigue crack growth resistance are essential features since the fatigue lifetime of aluminium components is dominated by the propagation of cracks and the determination of critical crack length under service loads is required in damage tolerant design. Therefore, these properties have been the subject of various investigations in literature [7, 10-12].

In a previous work by our research group [13], the tensile properties and high cycle fatigue behavior of AA7050 alloy treated for T6I4 (145°C/15min + 65°C/24h) were investigated and compared to those of the commercial temper T7451. Transmission electron microscopy analyses of strengthening precipitates were performed and the results showed that T6I4 treatment resulted in a higher volume fraction of smaller size precipitates. This microstructural feature was responsible by the improved ductility shown by T6I4 temper while maintaining the same levels of yield and ultimate tensile strength shown by T7451 condition. Moreover, the T6I4 temper condition presented higher strain hardening exponent when compared to T7451, indicating also a greater capacity to cyclic hardening, which was associated to a higher ability of dislocation pinning, loops formation and dislocation tangles configuration. The smooth samples rotating bending fatigue curves of both material conditions were similar. Nevertheless, the interrupted ageing led to improved notched fatigue resistance and hence lower notch sensitivity.

The aim of the present work was to evaluate the effects of the T6I4 treatment, with the same parameters adopted in the referred previous work [13], on the fracture toughness and fatigue crack growth behavior of AA7050 plate samples. The fracture toughness of the material in both T7451 and T6I4 conditions

was determined using the Chevron notch methodology. The fatigue crack growth tests were conducted under constant amplitude (R = 0.1) and variable amplitude loadings. In the former case, C(T) notched specimens in accordance to ASTM E647-15e1 standard were employed and the crack length was measured by the compliance method. In the latter case, hourglass shaped specimens were submitted to FALSTAFF spectrum loading with added marker blocks and the crack length was determined by quantitative fractography following the methods described in literature [12, 14-17].

MATERIAL AND METHODS

The present study was carried out on a commercial AA7050 alloy supplied in the form of a 75 mm thick rolled plate with T7451 temper. The chemical composition of the material, determined by optical emission spectrometry using a Shimadzu PDA-700 equipment, is (in wt.%): 5.58 Zn; 2.0 Cu; 1.88 Mg; 0.15 Zr; 0.07 Fe; 0.02 Si and Al balance. The interrupted aging condition (T6I4) was obtained from the as-received material by means of a solution treatment (485°C / 4h) followed by water quenching and two-step ageing (145°C / 30 min + 65°C / 24 h). The tensile properties and Vickers microhardness of the material conditions T7451 and T6I4, determined in a previous work [13], are given in Table 1, where σ_{YS} is the yield strength, σ_{UTS} is the ultimate tensile strength, ε is the total elongation, *RA* is the reduction in area, *K* and *n* are, respectively, the strength coefficient and the strain hardening exponent of the Ludwik's model for the true stress-strain curve and *HV* is the Vickers microhardness number. The specimens for the fracture toughness and fatigue crack growth (FCG) tests were produced by electrical discharge machining. All the mechanical tests in this work were performed at room temperature in laboratory air.

Table 1: Tensile properties and hardness of AA7050 temper conditions [13].

Temper	σ_{YS} *(MPa)*	σ_{UTS} *(MPa)*	ε *(%)*	*RA (%)*	*K (MPa)*	*n*	*HV*
T7451	470.0	531.1	10.8	21.9	710.7	0.0837	170
T6I4	472.8	561.0	19.4	36.8	808.5	0.1216	171

Chevron-Notch fracture toughness

Chevron-notched bar specimens with a width W = 47.6 mm, height $2H$ = 25.0 mm (i.e., $W/H \cong 3.8$) and slot angle $\varphi = 36°$ were adopted for this work. A pair of loading grips was machined from a SAE 4340 rod according to the design suggested by ASTM E1304 standard in order to clamp and apply a load to the mouth of the testpieces. The fracture toughness tests were conducted in an EMIC/INSTRON DL 10000 electromechanical testing machine, with a constant displacement rate of 0.2 mm/min. The mouth opening displacement was measured with an axial extensometer of 25 mm gage length coupled to the loading device at the specimen's surfaces positions. This test method has some advantages when compared to the conventional fracture toughness test, such as the initiation of a crack at very low loading level, the stable propagation through a considerably distance since its nucleation and the possibility of work with smaller specimens compared to those adopted by ASTM E-399 standard. The toughness values were based on the maximum force, following the method described in the Annex A1 of ASTM E1304 standard. The conditional K_{IvM} value, denoted by K_{QvM} was determined as a function of the dimensionless stress-intensity factor coefficient Y^* [18], the maximum load (P_M), the thickness (B) and the length (W) of the specimen, as shown by Eqn. 1. Three specimens of each material condition (T7451 and T6I4) were tested for this work. Fractographic analyzes were further performed using a FESEM Tescan Mira 3 microscope.

$$K_{QvM} = \frac{Y^* P_M}{B\sqrt{W}} \tag{1}$$

Constant amplitude fatigue crack growth

Compact tension C(T) specimens with thickness B = 4.5 mm, width W = 50.0 mm and 0.25 mm notch root radius, cut in the L-S orientation, were adopted for the constant amplitude FCG tests conducted in accordance with ASTM E647-15e1 standard. The tests were carried out under force control with load

ratio (min/max) R = 0.1 using a MTS 810 servo-hydraulic machine. The fatigue pre-cracking of the specimens was performed by letting a pre-crack to grow about 1.5 mm from the notch tip. The test frequency was kept constant at 5 Hz and the loading waveform was sinusoidal. The compliance method of crack length monitoring was used during the tests. The crack growth rate was calculated using the secant method.

Spectrum loading and quantitative fractography

Hourglass shaped coupons with a thickness of 5.0 mm and a corner notch of approximately 1.0 mm depth on one edge of the test section were adopted for the variable amplitude loading tests. The basic geometry and dimensions of the specimen is shown in Figure 1, resulting in a stress concentration factor $K_t \cong 1.06$. Since it is known that corner defects increase their size faster than surface and embedded cracks [19], this notch configuration was adopted in order to compare the behaviour of induced quarter elliptical cracks in the two studied aging conditions. The test specimens were subjected to a cyclic loading based on the standard industry FALSTAFF spectrum with added marker blocks to aid in the recognition of repeated spectrum blocks on the fracture surfaces by quantitative fractography [12, 14, 16, 17]. The so-called constant-amplitude marker bands consisted of 400 R = -1 cycles with normalized peak load level 0.5, divided by a single cycle between normalized load levels of -0.5 and 0.75. After the rupture of the specimens, quantitative fractography was performed using a motorized upright light microscope Zeiss AxioImager Z2m. Maps of the fracture surfaces were built using stacks of images captured under dark-field illumination. These stacks were pre-processed using the NIH ImageJ program [20] in order to track the progression marks produced by the marker bands, from which the crack sizes were determined by considering the origin at the notched corner of the rectangular cross section.

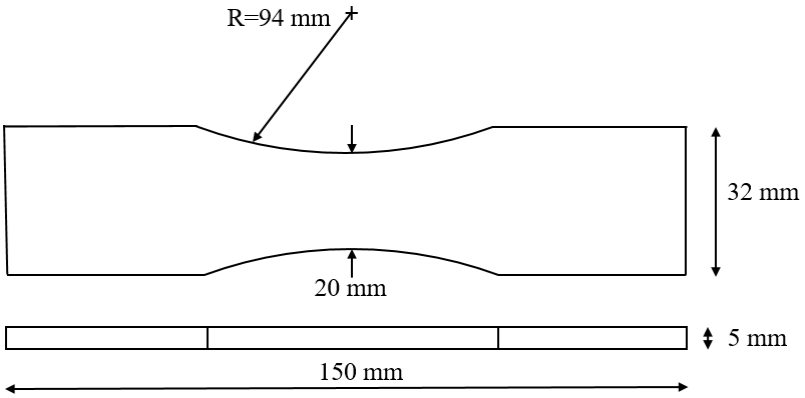

Figure 1: General geometry of the hourglass shaped test specimens.

RESULTS AND DISCUSSION

The results are presented and discussed emphasizing the comparison between the two material conditions (T7451 and T6I4) for each characteristic of their mechanical behavior evaluated in the tests.

Chevron-Notch fracture toughness

During the monotonic loading, all the specimens experienced sporadic crack extension behavior, showing sudden decreases in load accompanied by audible sound (pop-in). These discontinuous crack advances always resulted in less than 5% decrease in force, so that both material conditions can be said as presenting smooth crack growth behavior, as defined by ASTM E1304 standard. However, some differences were observed between the two material conditions. For instance, the applied force grew at a higher rate for T6I4 specimens as the displacement was imposed by the testing machine, resulting in higher loads for a given displacement. Moreover, the T7451 force-displacement graphs presented a well-defined maximum followed by a huge drop, whereas the T6I4 ones showed force growth up to final fracture. From the graphs, the maximum force (P_M) values were determined according to the method described in Annex A1 of ASTM E1304 standard (see Table 1). These values were employed in the

calculations of K_{QvM} according to Eqn. 1, the results of which are also shown in Table 1. For these calculations, the values of the dimensionless factor coefficient Y^* were determined by using an expression for short crack length [18], since that in all the tests the crack grew just 5 to 6 mm from the tip of the chevron-shaped ligament before the final rupture out of the chevron slots. Besides, because the actual crack surface deviated by more than $0.04B$ (the specimen thickness) for all the tests, the obtained K_{QvM} cannot be considered as valid K_{IvM} values according to ASTM E1304 standard, yet they can still be used to compare the chosen material conditions. The mean K_{QvM} values shown in Table 1 allow us to presume that the material's fracture toughness has significantly improved by T6I4 aging. Furthermore, the T7451 results are comparable to the amount 34.9 MPa·m$^{0.5}$ reported in literature [21].

Table 1: Chevron-notch fracture toughness test results.

AA7050	*T7451*		*T6I4*	
Test number	P_M (kN)	K_{QvM} (MPa·m$^{0.5}$)	P_M (kN)	K_{QvM} (MPa·m$^{0.5}$)
1	15.73	39.6	23.54	63.1
2	15.70	41.0	22.08	56.7
3	14.34	37.3	21.86	55.3
Sample mean	15.26	39.3	22.49	58.4

Although the specimens of both material conditions presented brittle fracture appearance from the macroscopic point of view, the fracture micro-mechanisms differed to some extent (see Figure 2). The T7451 specimen (a) presented cleavage facets, intergranular fracture and dimples preceding a secondary crack after which the fracture progressed predominantly by cleavage. The fracture surface of the T6I4 specimen (b) presented a more irregular topography, with a huge depression in the right side containing secondary cracks and followed by deformation lines. There are also shallow cavities and a lower portion of brittle characteristics, compared to the T7451 fracture.

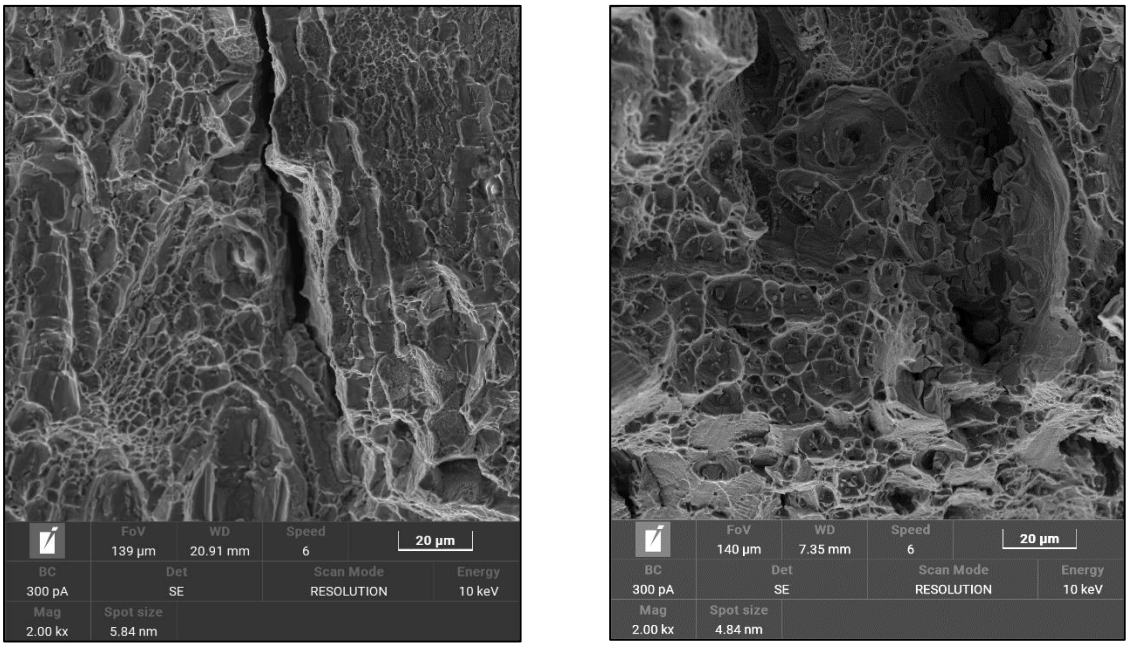

(a) (b)

Figure 2: SEM fractographs taken approximately 1.5 mm from the tip of the chevron notch of AA7050 specimens: (a) T7451, (b) T6I4 (crack growth direction: from left to right in both pictures).

Constant amplitude fatigue crack growth

The results of the constant amplitude fatigue tests are presented in terms of *da/dN vs. ΔK* plots (see Figure 3). For T7451 condition, the two specimens presented similar curves in the Paris region (stable regime), with *da/dN* ranging from 1-2 × 10^{-7} m/cycle at ΔK = 10 MPa·m$^{0.5}$ and from 7-9 × 10^{-7} m/cycle

at ΔK = 20 MPa·m$^{0.5}$, being comparable to literature results in this span [11, 22]. The pre-cracking of these specimens lasted 0.8 to 1.0 × 10^5 cycles. As for the T6I4 condition, crack initiation from notch tip required much more loading cycles. One of the specimens experienced crack arrest after nucleation and failed due to fretting fatigue from both holes after about 6.5 × 10^5 loading cycles. The pre-cracking stage of the other specimens was performed with higher K_{max} and, therefore, it was necessary to increase the maximum cycle force from 1.2 to 2.2 kN for running the tests. Even so, in one of the specimens the crack deviated from its ideal plane and the data acquisition was stopped (see Figure 3). The third specimen, despite showing a much higher apparent threshold compared to the T7451 ones, presented crack growth rate close to them at ΔK = 20 MPa·m$^{0.5}$. The pre-cracking lasted 2.52 × 10^5 cycles for this specimen. The T6I4 crack initiation issue may be related to a notch effect and is further discussed in the spectrum loading topic.

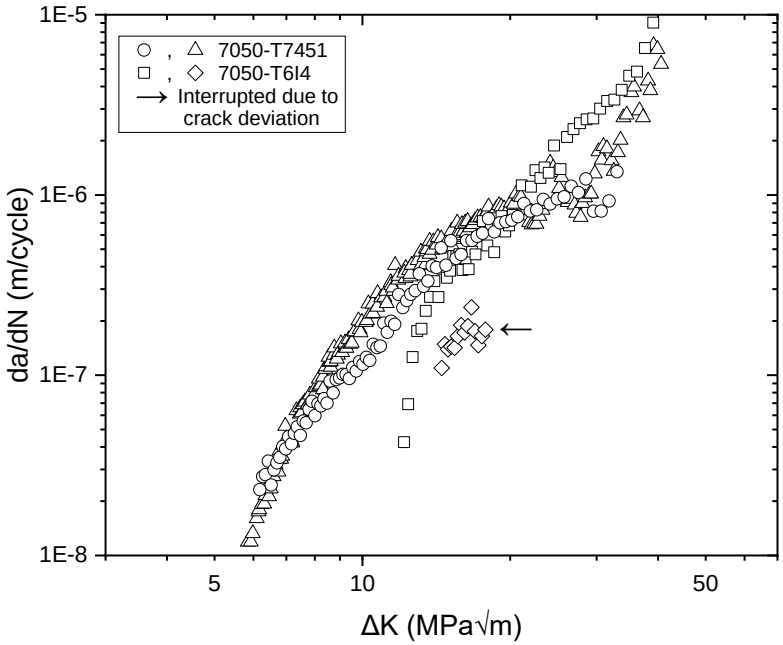

Figure 3: Constant amplitude (R = 0.1) fatigue crack growth curves for AA7050 alloy.

Spectrum loading

The fatigue lives of the spectrum loading specimens were 19 and 25 blocks for the T7451 condition tested at, respectively, 330 and 270 MPa stress levels, and 59 blocks for the T6I4 specimen tested at 330 MPa. The typical fracture appearance is shown in Figure 4, which is low magnification image mapping of the subcritical crack growth region.

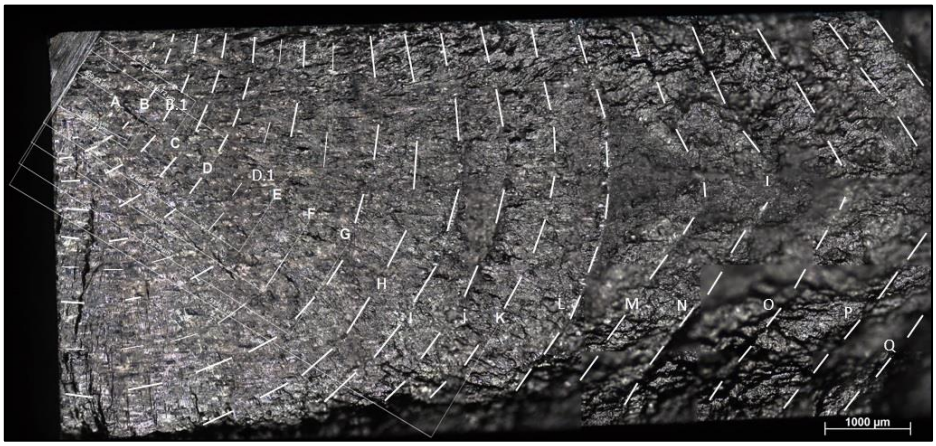

Figure 4: Fatigue fracture surface full view of the T7451 specimen tested at 270 MPa spectrum loading, with white lines indicating the crack front evolution.

After identifying the marker bands, their positions were measured at two points of the crack front. For the initially quarter-elliptical corner crack, measurements were taken of the semiaxis located on the face of the specimen (crack length) and at the intersection between the crack front and a 45° straight line drawn from the corner of the cross section (crack "depth"). As the cracks grew, their shape transitioned to a single-edge crack, and the measurements of the crack front were taken on the face (crack length) and at mid-thickness (crack "depth") of the cross section. The visible mark closest to the final rupture region was assumed to be due to the last loading block, and, therefore, the preceding marks were each associated with the corresponding previous block. Since the load spectrum consisting of 9006 cycles represents 100 equivalent flight hours [23], the experimental crack growth histories were obtained by plotting the crack size data against flight hours (see Figures 5 and 6).

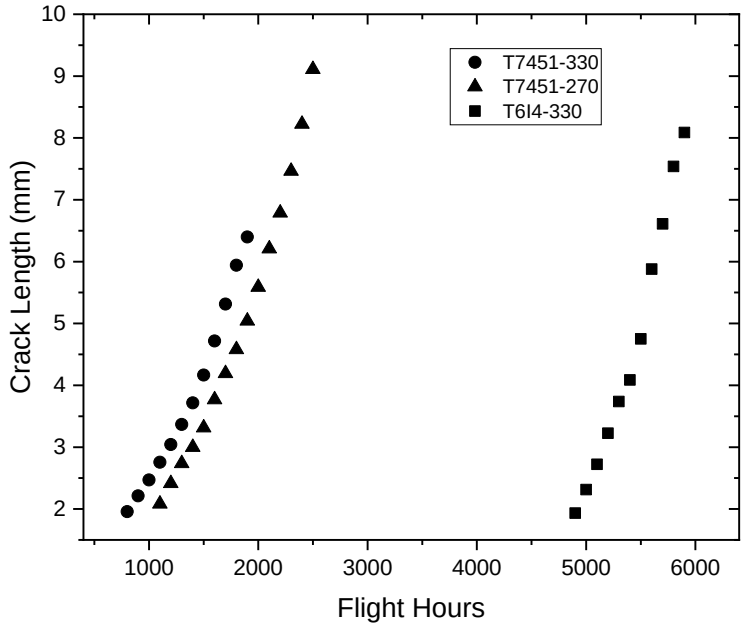

Figure 5: Spectrum loading fatigue crack growth data, derived from quantitative fractography.

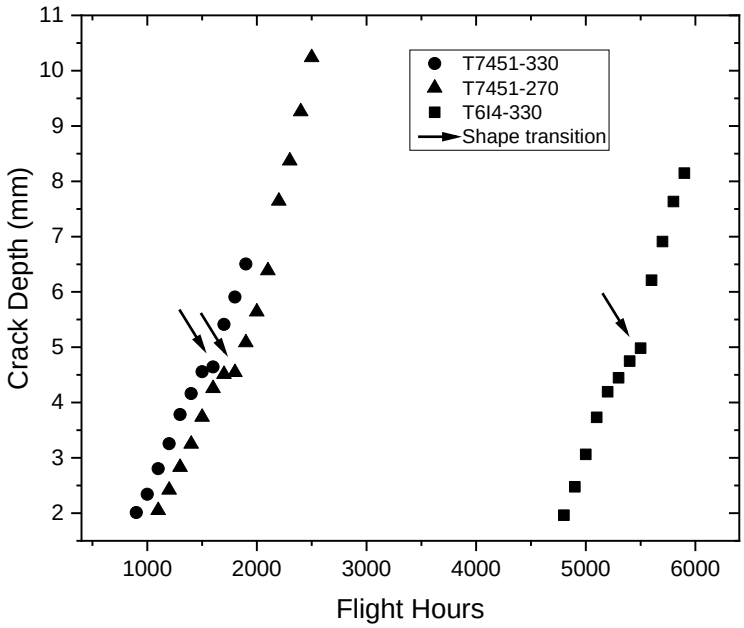

Figure 6: Spectrum loading fatigue crack growth data, derived from quantitative fractography.

Not enough clear marks were observed in the vicinity of the notch root, so the early crack growth history was not registered in the graphs of Figures 5 and 6. A more accurate comparison of the macro crack growth histories is made by disregarding the equivalent flight hours spent in the nucleation stage and translating the curves to the same initial point (see Figures 7 and 8). In such manner, it can be seen that the crack grew somewhat faster in the T6I4 specimen than in the T7451 one loaded at the same level. It is also worth noting that no significant variation of crack growth was observed between T7451 specimens, except for the fact that the higher propagation life shown by the specimen tested at 270 MPa stress level seems to be more related to its larger crack size before final rupture. Nevertheless, the most remarkable finding was the aforementioned higher number of loading blocks withstood by the T6I4 specimen (59 blocks) in comparison to the T7451 ones (19 and 25). From Figures 5 to 8 it became clear that the life increase provided by the interrupted aging was due to a much higher number of loading blocks spent during nucleation and early crack propagation.

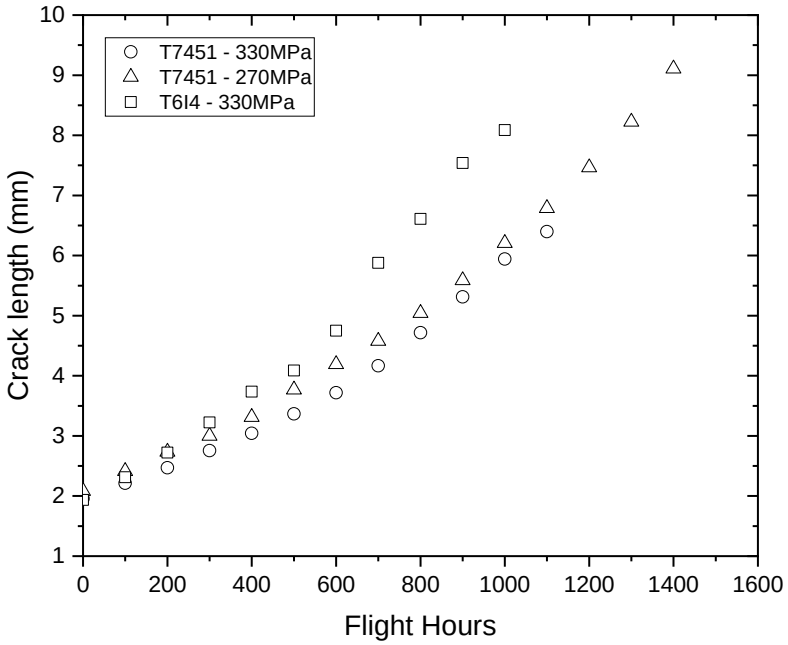

Figure 7: Spectrum loading fatigue crack growth data, translated to a common starting point.

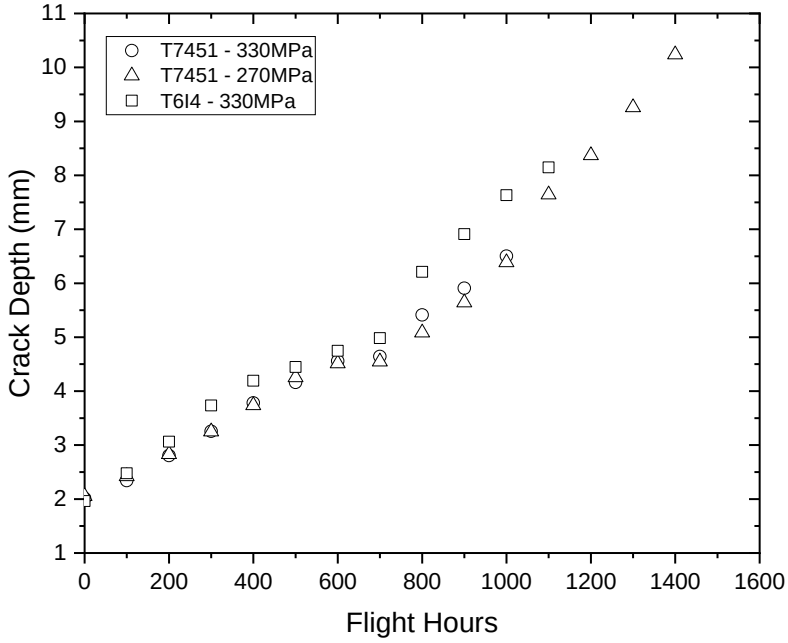

Figure 8: Spectrum loading fatigue crack growth data, translated to a common starting point.

In both constant amplitude and variable amplitude fatigue tests, the significant difference between T6I4 and T7451 conditions occurred during the nucleation and early crack propagation stages. It is known from literature [24, 25] that, when a tensile fatigue crack emanates from a notch, the initial growth of the nascent crack may be affected and even completely arrested by the plastic deformation occurring at the notch root. This transient effect, whose intensity depends on material, is usually exhibited by a small flaw until its tip is relieved from the strain field associated with the notch root deformation. In a previous paper [13], it was shown that AA7050-T6I4 notched specimens tested under rotary bend loading presented higher fatigue resistance and lower notch sensitivity than T7451 ones. The results obtained in the present paper evince that those rotary bend results are due to the transient notch effect and unrelated to the fatigue macro-crack growth behavior of T6I4 condition.

CONCLUSION

This work presented results of chevron notch fracture toughness and fatigue crack propagation tests carried out on samples of AA7050 alloy with two temper conditions: T7451 and T6I4. In the fracture toughness tests, the non-pre-cracked T6I4 specimens achieved higher loads as the crack nucleated and grew from the notch tip, resulting in higher K_{QvM} mean values (58.4 MPa·m$^{0.5}$) than T7451 ones (39.3 MPa·m$^{0.5}$). The fatigue crack growth behavior of these material conditions under both constant amplitude (R = 0.1) and variable amplitude (FALSTAFF spectrum) loadings was found to be nearly similar. However, the higher apparent threshold observed in the constant amplitude tests and higher fatigue life presented by the T6I4 specimen under spectrum loading lead us to conclude that this material condition is more prone to the transient notch effect that retards the initial growth of a nascent crack. This effect is not manifested for a large crack, when the plastic zone is small compared to the extent of the elastic stress field ahead of the crack tip and the stress intensity factor K is the sole driving force for crack growth. On the other hand, the higher ability of AA7050-T6I4 to accumulate plastic deformation, which is related to the favorable combination of higher ductility and strain hardening exponent exhibited by this material condition, acts in favor of retarding the crack nucleation and early growth from a notch.

REFERENCES

[1] Dursun, T. and Soutis, C. (2014), *Materials & Design*, vol. 56, p. 862.
[2] Buha, J., Lumley, R.N. and Crosky, A.G. (2008), *Mater. Sci. Engng. A*, vol. 492, p. 1.
[3] Totten, G. E. and Mackenzie and D. S. (2003). *Handbook of aluminum*, New York: Physical Metallurgy and Process, vol.1, p. 169.
[4] Dumont, D., Deschamps, A. and Brechet, Y. (2003), *Mater. Sci. Engng. A*, vol. 356, p. 326.
[5] Jiang, F., Zurob, H.S., Purdy, G.R. and Zhang, H. (2016), *Mater. Charact.*, vol. 117, p.47.
[6] Chen, J., Zhen, L., Yang, S., Shao and W., Dai, S. (2009), *Mater. Sci. Engng. A*, vol. 500, p. 34.
[7] Han, N., Zhang, X., Liu, S., Ke, B. and Xin, X. (2011), *Mater. Sci. Engng. A*, vol. 528, p. 3714.
[8] Nandana, M.S., Bhat, K.U. and Manjunatha, C.M. (2019), *Proc Struct Integrity*, vol. 14, p. 314.
[9] Carvalho, A.L.M., Renaudin, L.B., Zara, A.J. and Martins, J.P. (2022), *J. Alloys Compd*, vol. 907, p. 164400.
[10] Bianchetti, C., Zheng, R., Chromik, R.R., Lévesque, M. and Brochu, M. (2018), *Eng Fract Mech*, vol. 202, p. 20.
[11] Wang, Y.L., Pan, Q.L., Wei, L.L., Li, B. and Wang, Y. (2014), *Mater Des*, vol. 55, p. 857.
[12] Jones, R. Molent, L. and Barter, S. (2013), *Int. J. Fatigue*, vol. 55, p. 178.
[13] Antunes, A.M.B.S., Baptista, C.A.R.P., Barboza, M.J.R., Carvalho, A.L.M. and Mogili, N.V.V. (2019), J Braz Soc Mech Sci, vol. 41, p. 319.
[14] Molent, L., Sun, Q. and Green, A.J. (2006), *Fatigue Fract Engng Mater Struct*, vol. 29, p. 916.
[15] Tamboli, D., Barter, S. and Jones, R. (2018), *Int. J. Fatigue*, vol. 109, p. 10.
[16] Dixon, B. and Barter, S. (2008). *Comparison of the Spectra Applied to the FT55 and FINAL Full-scale F/A-18 Fatigue Tests, DSTO-TR-2170*, Defence Science and Technology Organisation, Melbourne.

[17] Barter, S.A and Wanhill, R.J.H. (2009). *Marker loads for quantitative fractography of fatigue cracks in aerospace alloys*, *NLR-TP-2008-833*, National Aerospace Laboratory, Amsterdam.
[18] Munz, D., Bubsey, R.T. and Srawley, J.E. (1980), *Int Journ of Fracture*, vol. 16, p. 359.
[19] Toribio, J., Matos, J.C. and González, B. (2017), *Appl. Sci.*, vol. 7, p.746.
[20] Schneider, C.A., Rasband, W.S. and Eliceiri, K.W. (2012), *Nat Methods*, vol. 9, p. 671.
[21] Tsuchida, T., Niinomi, M., Ibaragi, M., Yoshida, H., Okada, K., Miura, Y. and Kanno, M. (1998). In: *Aluminum Alloys*, Proceedings of the 6th International Conference on Aluminum Alloys, vol. 3, pp. 1343-1348, The Japan Institute of Light Metals, Tokyo.
[22] Jesus, J.S., Antunes, F.V., Prates, P., Branco, R., Antunes, P.V., Borrego, L.P. and Simões Neto, D.M. (2022), *Int. J. Fatigue*, vol. 164, p. 107136.
[23] Hu, W., Krieg, B. and Torregosa, R. (2014), *Adv Mat Res*, vols. 891-892, p. 1197.
[24] Suresh, S. (2001). *Fatigue of Materials*, Cambridge University Press, Cambridge, 679 p.
[25] Smith, R.A. and Miller, K.J. (1978), *Int. J. Mech. Sci.*, vol. 20, p. 201.